Design and Prototyping of BiSoft.Q, A 3-D Printed Bi-directional Deformable Actuator

Design and Prototyping of BiSoft.Q, A 3-D Printed Bi-directional Deformable Actuator

Giovanni Colucci(✉), Simone Duretto, and Giuseppe Quaglia

Department of Mechanical and Aerospace Engineering, Politecnico di Torino, Corso Duca degli Abruzzi 24, 10129 Torino, Italy
{giovanni_colucci,giuseppe.quaglia}@polito.it,
simone.duretto@studenti.polito.it

Abstract. The paper presents the design guidelines and early prototyping of a 3-D printed pressure-driven deformable actuator that can actively contract and expand. The actuator is entirely realized through FDM (Fused Deposition Modelling) technologies and affordable materials. The basic working principle of the actuator is presented and its functional design is supported by preliminary considerations and final design guidelines. Additional information about the first prototype and a few practical details are provided.

Keywords: Soft Robotics · Fluidic Actuator · Pleated Pneumatic Artificial Muscle · Pneumatic Actuator

1 Introduction

In recent times, the use of additive manufacturing technologies had lead to the birth of novel pressure-driven deformable actuators, where the properties of highly flexible materials are combined with the possibility to print even complex and intriguing geometries [1]. The main features of those deformable actuators, also called *soft actuators* due to their marked elasticity [2], are the compliant behaviour and the low weight [3,4]. The idea of those devices was first introduced with the PAMs (Pneumatic Artificial Muscles), that are deformable actuators that converts pneumatic powers into pulling forces [5], mainly characterized for their high force-weight ratio, minimal compressed air consumption and no mechanical friction and wear, which result into an overall actuation energy saving.

This paper presents the design and prototyping of BiSoft.Q, a soft actuator that can exert both a push or a pull force using two antagonistic internal chambers. The prototype of the actuator is showed in Fig. 1.

The basic principle of the actuator, i.e. the use of two antagonistic chambers (Fig. 2) and the fundamental properties of both the internal and external membrane, is inspired by the BiFac actuator presented by Ferraresi et al. in

M. Okada (Ed.): IFToMM WC 2023, MMS 149, pp. 710–720, 2024.
https://doi.org/10.1007/978-3-031-45709-8_69

[6], where reinforcement longitudinal fibers make the membrane anisotropic as regards the force transmission and deformation. In this case, the actuator was nonetheless realized with different geometry of the external membrane and also different technological solutions. The geometry of the external membrane is similar to what already explored by the PPAMs (Pleated Pneumatic Muscles) [7], where the concept of material rearranging was first introduced to avoid material deformation and membrane stresses.

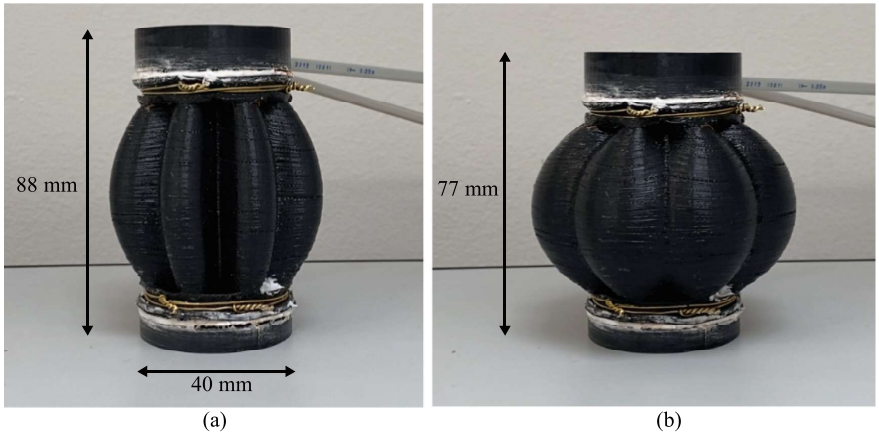

Fig. 1. The bi-directional deformable actuator in the two extreme configurations. (a) Completely stretched. (b) Completely contracted.

The use of a pleated geometry to facilitate and drive the actuator reconfiguration was also presented by De pascali et al. in [8], where numerical methods are exploited and the bidirectionally of the actuator is obtained with a single working chamber that is nevertheless connected to a compressor or a vacuum pump. The main novelties of this paper are the implementation of a completely analytical model to estimate the actuator stroke and its related actuation forces, and the implementation of two antagonistic chambers to avoid the use of a vacuum pump.

1.1 Actuator Working Principle

BiSoft.Q is formed by two membranes, a pleated external shell and an internal bellows, that form two chambers that can be connected to different pressure levels (Fig. 2). Figure 3 shows a schematic representation of the actuator in two different configurations, described by the longitudinal position variable x. Please note how x is measured starting from the actuator printed configuration, and a positive value of x is related to an elongation, while a negative one is related to a contraction. The term *active chamber* refers to the chamber at the higher pressure level.

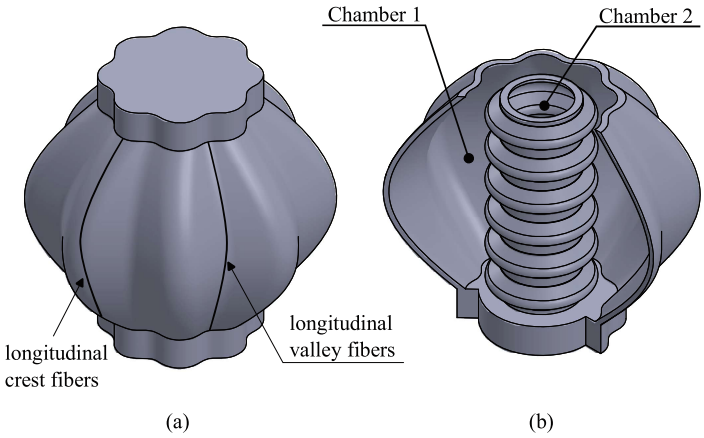

Fig. 2. (a) The external pleated surface. (b) A section showing the internal chambers of the actuator.

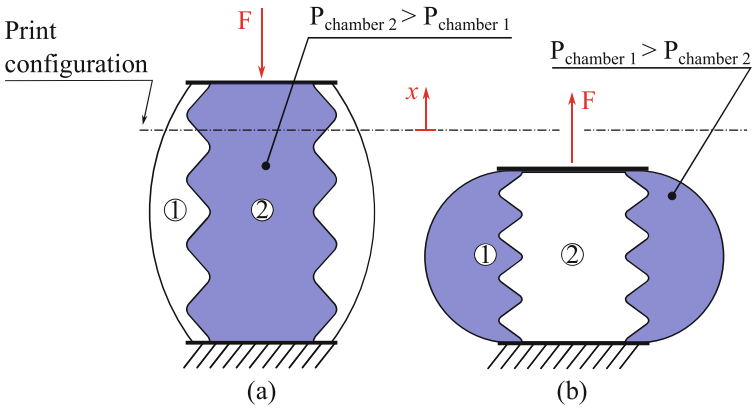

Fig. 3. A schematic representation of a longitudinal section of the actuator in two arbitrary configurations. (a) Chamber 2 is active, $F < 0$. (b) Chamber 1 is active, $F > 0$.

2 Design Methods

Within the present section, an analytic method is exploited to obtain a few effective design guidelines, basing on the following physical values:

- The actuator stroke s defined as $s = x_{max} - x_{min}$, where $x_{max,min}$ represent respectively the maximum and minimum longitudinal position of the actuator.
- F, i.e. the force that is exerted on the actuator by the environment, defined positive accordingly to Fig. 3.

This method is especially addressed towards the external pleated shell and its design parameters, assuming the internal bellows geometry can be adapted afterwards. This choice depends on the intrinsic geometrical complexity of the external membrane, and also because it strongly affects the actuator performance.

The actuator geometry is entirely described by means of the design parameters presented in Fig. 4. Starting from the cross-section B-B, placed at an height of $L/2$ from O along the k axis, the primitive curve that generates the pleats is formed by a first arc (I), a tangent segment (II) and a second arc (III). The primitive curve is thus flipped along the i axis, thus the resulting curve is repeated N times to create a circular pattern that is centered in O'.

The entire shell is created by making a loft extrusion of the above described curve along the k axis. The guide curve is an arc in the longitudinal plane $< i, k >$ centered in C, that guides the valley longitudinal fibers in Fig. 2(a). The chosen geometrical design parameters are:

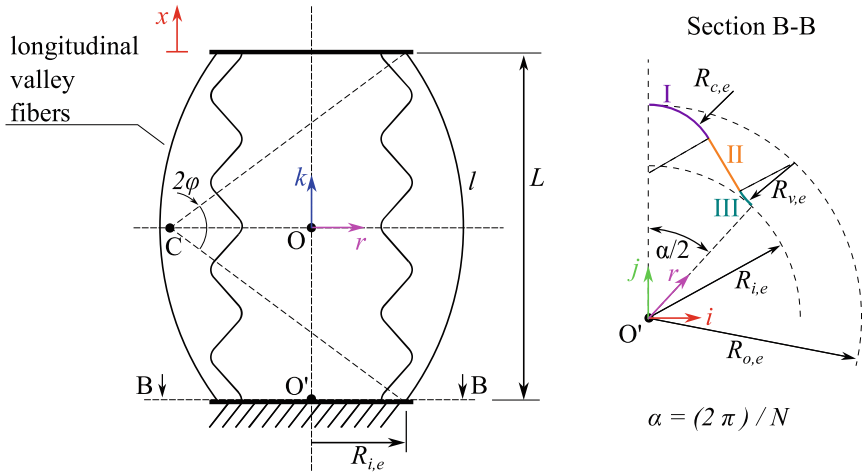

Fig. 4. Representation of the internal bellows and external pleated shell. All the chosen geometrical parameters are reported.

- l the length of the valley longitudinal fibers when printed;
- L the longitudinal height of the actuator when printed;
- $R_{i,e}$ the radius of the arc constructed by intersecting the valley longitudinal fibers with the B-B section plane;
- N the number of pleats;
- $R_{o,e}$ similarly to $R_{i,e}$ it represents the arc on which the crest longitudinal fibers intersect the B-B section plane;
- $R_{[c,v],e}$ respectively the crest and valley arc radius of the primitive curve on the B-B plane.

2.1 Preliminary Assumptions

The design procedure is based on the following simplifying assumptions. Some of them are similar to what presented in [6]:

- The longitudinal fibers of the external pleated shell can be treated as infinitely rigid during the actuator elongation, i.e. the longitudinal elasticity of the shell is neglected;
- The circumferential fibers of the internal bellows, in a similar manner to what explained for the external shell, do not undergo a circumferential deformation;
- The valley longitudinal fibers are considered the main accountable for the load transmission when chamber 1 is active, i.e. the the pressure force that acts upon the n-th pleat is counterbalanced by the tension of those fibers;
- The symmetric properties of the external shell can be used to estimate its deformed configuration as a function of the actuator elongation x. Moreover, the minimum elongation x_{min} is reached when the valley longitudinal fibers showed in Fig. 4 take the shape of a semi circle;
- The border effects that arise from the mechanical rigid mounting between the two shells and the terminal plates are neglected.

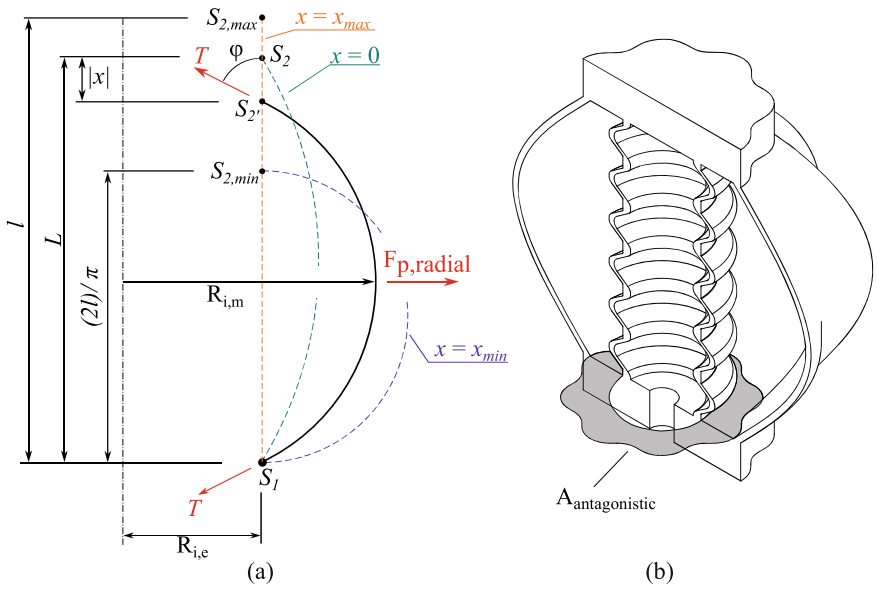

Fig. 5. (a) Longitudinal valley arc under deformation. The pressure force $F_{p,radial}$ on each pleat is counterbalanced from the fiber tension T. (b) Representation of the area that generates an antagonistic pressure force when the chamber 1 is active.

2.2 Stroke Evaluation

Thus, the theoretical longitudinal stroke of the external pleated shell can be estimated by referring to Fig. 5 (a) as:

$$s = x_{max} - x_{min} = (l - L) - \left(\frac{2\,l}{\pi} - L\right) = l\left(1 - \frac{2}{\pi}\right) \approx 0.36\,l \tag{1}$$

which correspond respectively to the configuration where the longitudinal fiber is entirely straight and the configuration where it forms an arc that is tangent to both the upper and lower terminal plates. Since the longitudinal fibers are considered as non-extensible, the valley arc length l remains constant during the elongation and contraction phases. Moreover, by considering the point S_1 as fixed, S_2 translates of a quantity of x along the k axis. The angle $\varphi = \varphi(x)$ between a line tangent to the valley arc in $S_{2'}$ and the k axis can be obtained by geometrical considerations:

$$\frac{\varphi}{sin(\varphi)} = \frac{l}{L + x} \tag{2}$$

which can not be solved analytically. Please note how $\varphi \in [0, \pi/2]$ where the boundary values are reached for a value of x of respectively $x = x_{max}$ and $x = x_{min}$.

2.3 Force Evaluation

Consider the chamber 2 as the active one and pressurized at a pressure level $P_2 > P_1$. By assuming $P_1 = P_{atmospheric}$ and by neglecting the elastic membrane forces of both the internal and external shell, the F formulation trivially becomes:

$$F = (P_2 - P_{atm})\,\pi\,R_{i,e}^2 \tag{3}$$

where it was assumed $R_{i,e}$ as the radius of the terminal plate of the internal bellows, which is both beneficial when chamber 1 or 2 is active, as it will be further explained. By considering the chamber 1 as active instead, since the valley longitudinal fibers of Fig. 2 are considered as the main responsible for the strain transmission, the tension force T on each longitudinal fiber can be calculated as:

$$T = \frac{F_{p,radial}(x)}{2\,sin(\varphi(x))} \tag{4}$$

where $F_{p,radial}$ is the resulting pressure force that acts on the n-th pleat. Thus, F can be computed by imposing the force equilibrium on the terminal plate of the actuator:

$$F(x) = N\,\frac{F_{p,radial}(x)}{2\,\tan(\varphi)} - F_{antagonistic} - F_{elastic}(x) \tag{5}$$

where the first term comes from Eq. (4), now considering the total number of N pleats; the second term considers the antagonistic force that acts upon the

$A_{antagonistic}$ area showed in Fig. 5 (b), while the latter term considers the elastic return force of both the internal and external membrane, that is nonetheless neglected. As cited before, to reduce $F_{antagonistic}$, a radius of the terminal plate of the internal bellows about equal to $R_{i,e}$ is encouraged.

$F_{p,radial}$ is calculated by defining the geometry of the n-th pleat as a surface that is function of the variables $(\vartheta_1, \vartheta_2)$, as showed in Fig. 6:

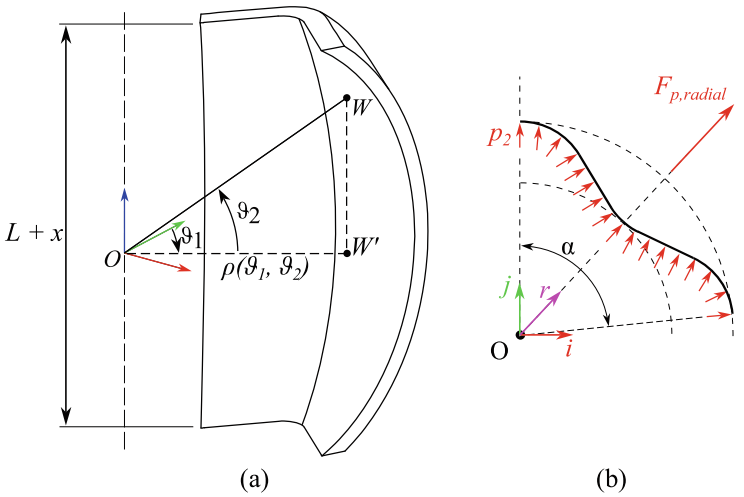

Fig. 6. (a) Representation of $OW = OW(\vartheta_1, \vartheta_2)$. (b) Resultant force $F_{p,radial}$ acting on the n-pleat.

$$\underline{\Sigma}(\vartheta_1, \vartheta_2) = OW(\vartheta_1, \vartheta_2) = X(\vartheta_1, \vartheta_2)\hat{i} + Y(\vartheta_1, \vartheta_2)\hat{j} + Z(\vartheta_1, \vartheta_2)\hat{k} \tag{6}$$

The vector $\hat{n}$, that is normal to the surface in P is defined as:

$$\hat{n}(\vartheta_1, \vartheta_2) = (n_i, n_j, n_k) = -\frac{\dfrac{\partial \underline{\Sigma}}{\partial \vartheta_1} \times \dfrac{\partial \underline{\Sigma}}{\partial \vartheta_2}}{\left\| \dfrac{\partial \underline{\Sigma}}{\partial \vartheta_1} \times \dfrac{\partial \underline{\Sigma}}{\partial \vartheta_2} \right\|} \tag{7}$$

Thus, the total pressure force acting on the n-th pleat can be computed as:

$$\underline{F_p} = \int_{\Sigma} p\hat{n} d\Sigma = \int_0^{\alpha} \int_{-\vartheta_{2,max}}^{\vartheta_{2,max}} p\hat{n} \left\| \frac{\partial \underline{\Sigma}}{\partial \vartheta_1} \times \frac{\partial \underline{\Sigma}}{\partial \vartheta_2} \right\| d\vartheta_1 d\vartheta_2 \tag{8}$$

where $p = P_1 - P_{atm}$. Please note how, due to the geometric symmetry of the pleat, the component of F_p along k axis is null. The two components along i and j produce instead a total force that acts radially to the membrane:

$$F_{p,radial} = \sqrt{F_{p,i}^2 + F_{p,j}^2} \tag{9}$$

2.4 Results

Basing on the methods above presented, the authors selected a few considerations that can act as design guidelines:

- The length of the valley fibers l can be chosen as a function of the desired stroke s, as showed in Eq. (1);
- L, i.e. the longitudinal height of the actuator when printed, does not affect its stroke or exerted force F. It can be instead chosen depending on the desired rest configuration of the actuator, choosing a value ranging between:

$$\frac{L}{l} \in [2/\pi\ ,\ 1] \tag{10}$$

  where the lower bound leads to a printed geometry close to the entire compressed configuration, while the upper bound leads to an actuator that is entirely stretched.
  It is worth noticing that, if FDM (Fused Deposition Modelling) fabrication techniques are employed, a minimum overhang value of about 40 deg must be guaranteed [9] to prevent from membrane damages and gaps. To this aim the maximum value of φ defined in Fig. 5 (a) is $\varphi(x=0)_{max} = 50$ deg, which leads to a lower constraint on the L value:

$$\left(\frac{L}{l}\right)_{min} \approx 0.85 \tag{11}$$

- The internal bellows should be mounted close to the external pleated membrane to reduce the value of $F_{antagonistic}$ of Eq. (5) when chamber 1 is active, and also to increase F when chamber 2 is active.
  In Fig. 7, for instance, the estimated behaviour of $F(x)$ is presented for a fixed value of l and a value of $R_{i,e}$ spanning between 15 up to 40 mm. Those kind of actuators, with a geometrical ratio $l\,/(2\,R_{i,e})$ from approximately 0.8 up, are evidently marked by higher values of F when chamber 1 is active. Please notice $F < 0\ \forall x \in [x_{min}, x_{max}]$ when chamber 2 is active since F represents the force exerted on the actuator by the environment under equilibrium condition.
- The remaining geometrical parameters N, $R_{o,e}$ and the two radius lengths $R_{[c,v],e}$ present no significant effect on the evaluated physical values x and F. Thus it is suggested to choose them mostly on the basis of technological issues instead of model-based considerations.
  In detail, the choice of $R_{o,e}$ value should be done to allow the correct deformation of the actuator when chamber 1 is active. Indeed, by referring to Fig. 1 (b), this phase is characterized by a progressive enlarging of the valley fibers until they reach the crest fibers. By referring to $R_{i,m}(x)$ and $R_{o,m}$ as respectively the valley and crest circle radii on the median cross-section of the actuator in Fig. 5 (a), it can be easily obtained that:

$$R_{i,m}(x = x_{min}) = R_{i,e} + \frac{l}{\pi} \tag{12}$$

where $R_{i,e}$ is assumed as fixed. The configuration with $x = x_{min}$ is obtained when the longitudinal crest fibers take the form of a semi circle with $\varphi(x = x_{min}) = \pi/2$, as underlined within the simplifying assumptions. Thus, it seems reasonable to assume a value of $R_{o,m}$ slightly bigger than $R_{i,m}(x = x_{min})$. This choice can be therefore used to mathematically obtain the desired value of $R_{o,e}$.

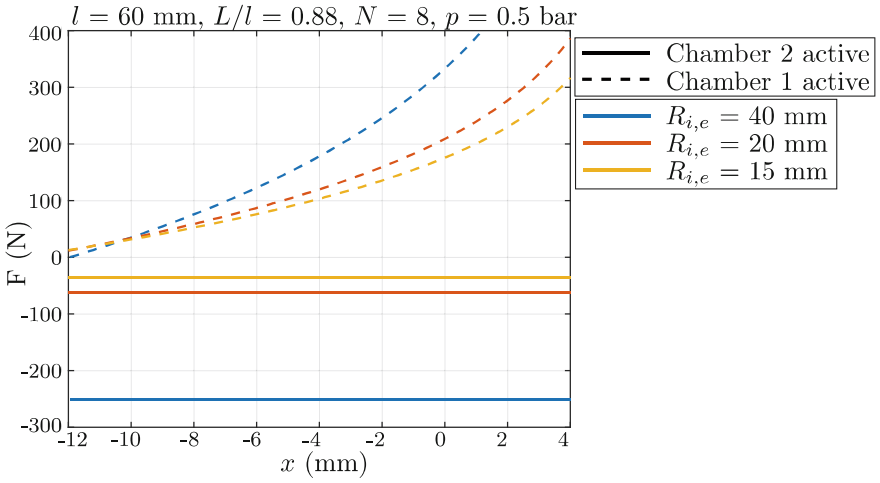

Fig. 7. Estimated forces with $l/(2\,R_{i,e})$ ranging between $[0.75, 2]$.

3 Prototyping

To enhance the potential to print those kind of actuators with affordable materials and equipment, a first version of BiSoft.Q was entirely produced through FDM methods with an Ultimaker Cura S5 printer. An exploded view of the actuator is presented in Fig. 8.

The upper and lower rigid cap were realized in standard plastic material, with inner canals for the air inflation. The two caps hold both the internal bellows and the external pleated surface with geometrical mechanical couplings, and two metallic clamping rings are used on the outer face of the pleated shell to prevent from air leakages when chamber 1 is active.

The two deformable membranes were instead fabricated in Filaflex 60A Pro, a Thermoplastic Polyether-Polyurethane with a tensile strength of 26 MPa and an elongation at break of 950%. The high elasticity of this material guarantees low elastic return forces, but it resulted as very vulnerable to gauge pressure level higher than 0.7 bar.

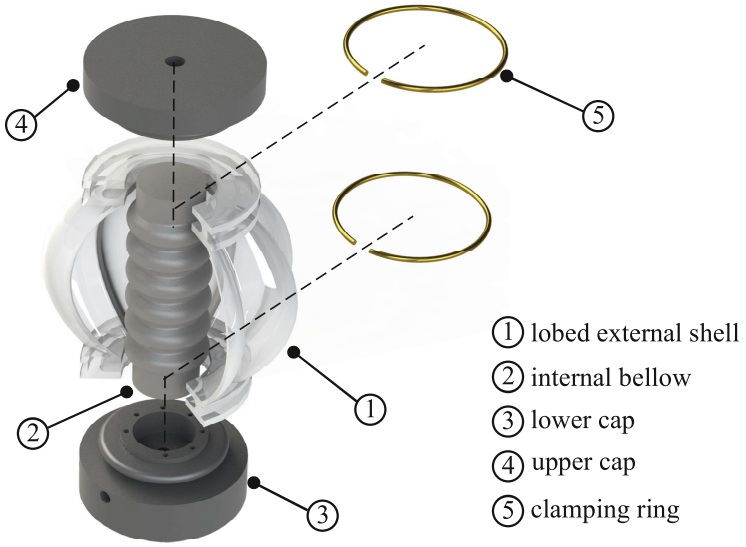

Fig. 8. Exploded view of the actuator prototype.

Those kind of geometries have been printed also guaranteeing the absence of major air leakages. The eventual presence of minor air damages, that could arise especially if the pleated shell is printed with a value of L/l less than what presented in Eq. (11), were fixed with the use of a commercial silicone sealant (in white in Fig. 1).

Thanks to its modular design, the actuator can be easily disassembled to check for eventual damages of the internal bellows.

4 Conclusions

This paper presents BiSoft.Q, a 3-D printed pressure-driven bi-directional actuator, that works on the counter action of two pressurized internal chambers. An analytical method was exploited for design purposes, to underline the significant effect of the design parameters on the actuator estimated performance. A first prototype, that can be disassembled, was realized with a commercial TPU 60A for the deformable membranes. The possibility to dismount the actuator allows to check eventual internal damages, that often affect those kind of soft systems.

As further developments, experimental tests of the actuator performance will be performed to validate the analytical model.

Acknowledgment. The research activity was supported by Pic4Ser-PoliTO Interdepartmental Centre For Service Robotics. https://pic4ser.polito.it/ (accessed on 27 April 2023).

References

1. El-Atab, N., Mishra, R.B., Al-Modaf, F., Joharji, L., Alsharif, A.A., Alamoudi, H., Diaz, M., Qaiser, N., Hussain, M.M.: Soft actuators for soft robotic applications: a review. Adv. Intell. Syst. 2(10), 2000,128 (2020). https://doi.org/10.1002/aisy.202000128
2. Tauber, F., Desmulliez, M., Piccin, O., Stokes, A.A.: Perspective for soft robotics: the field's past and future. Bioinspiration Biomimetics 18(3), 035,001 (2023). https://doi.org/10.1088/1748-3190/acbb48
3. Daerden, F., Lefeber, D.: Pneumatic artificial muscles: actuators for robotics and automation. Eur. J. Mech. Environ, Eng (2002)
4. Terryn, S., Brancart, J., Lefeber, D., Assche, G.V., Vanderborght, B.: Self-healing soft pneumatic robots. Sci. Robot. 2(9), eaan4268 (2017). https://doi.org/10.1126/scirobotics.aan4268
5. Wickramatunge, K.C., Leephakpreeda, T.: Empirical modeling of dynamic behaviors of pneumatic artificial muscle actuators. ISA Trans. **52**(6), 825–834 (2013). https://doi.org/10.1016/j.isatra.2013.06.009
6. Ferraresi, C., Franco, W., Quaglia, G.: A novel bi-directional deformable fluid actuator. Proc. Inst. Mech. Eng. C J. Mech. Eng. Sci. 228(15), 2799–2809 (2014). https://doi.org/10.1177/0954406214522022
7. Daerden, F., Lefeber, D.: The concept and design of pleated pneumatic artificial muscles. Int. J, Fluid Power (2014)
8. Pascali, C.D., Naselli, G.A., Palagi, S., Scharff, R.B.N., Mazzolai, B.: 3D-printed biomimetic artificial muscles using soft actuators that contract and elongate. Sci. Rob. 7(68), eabn4155 (2022). https://doi.org/10.1126/scirobotics.abn4155.
9. Jiang, J., Stringer, J., Xu, X., Zhong, R.Y.: Investigation of printable threshold overhang angle in extrusion-based additive manufacturing for reducing support waste. Int. J. Comput. Integr. Manuf. **31**(10), 961–969 (2018). https://doi.org/10.1080/0951192X.2018.1466398